CSIRO PUBLISHING

International Journal of Wildland Fire
https://doi.org/10.1071/WF17177

Time series of high-resolution images enhances efforts to monitor post-fire condition and recovery, Waldo Canyon fire, Colorado, USA

Melanie K. Vanderhoof[A,B], *Clifton Burt*[A] *and Todd J. Hawbaker*[A]

[A]US Geological Survey, Geosciences and Environmental Change Science Center, PO Box 25046, DFC, MS980, Denver, CO 80225, USA.
[B]Corresponding author. Email: mvanderhoof@usgs.gov

Abstract. Interpretations of post-fire condition and rates of vegetation recovery can influence management priorities, actions and perception of latent risks from landslides and floods. In this study, we used the Waldo Canyon fire (2012, Colorado Springs, Colorado, USA) as a case study to explore how a time series (2011–2016) of high-resolution images can be used to delineate burn extent and severity, as well as quantify post-fire vegetation recovery. We applied an object-based approach to map burn severity and vegetation recovery using Worldview-2, Worldview-3 and QuickBird-2 imagery. The burned area was classified as 51% high, 20% moderate and 29% low burn-severity. Across the burn extent, the shrub cover class showed a rapid recovery, resprouting vigorously within 1 year, whereas 4 years post-fire, areas previously dominated by conifers were divided approximately equally between being classified as dominated by quaking aspen saplings with herbaceous species in the understorey or minimally recovered. Relative to using a pixel-based Normalised Difference Vegetation Index (NDVI), our object-based approach showed higher rates of revegetation. High-resolution imagery can provide an effective means to monitor post-fire site conditions and complement more prevalent efforts with moderate- and coarse-resolution sensors.

Additional keywords: burned area, GeoEye-1, Landsat, QuickBird-2, revegetation, severity, Wildfire, Worldview-2, Worldview-3.

Received 20 December 2017, accepted 21 August 2018, published online 7 September 2018

Introduction

Fire is an important driver of change and ubiquitous in almost all terrestrial ecosystems (Giglio *et al.* 2013; Sommers *et al.* 2014). Using remotely sensed imagery to monitor patterns of fire, burn severity and vegetation recovery can inform efforts to track fire-induced changes to biomass and species distribution (Bond *et al.* 2005; Goetz *et al.* 2005), nutrient cycling (Conard *et al.* 2002; Bond-Lamberty *et al.* 2007), greenhouse gas emissions (Palacios-Orueta *et al.* 2005; Randerson *et al.* 2005) and landscape heterogeneity (Parisien *et al.* 2006; Hayes and Robeson 2011). Efforts to map fire extent and post-fire recovery have been dominated by coarse-resolution sensors such as the Advanced Very High Resolution Radiometer (AVHRR) (Moreno-Ruiz *et al.* 2014), Moderate Resolution Imaging Spectroradiometer (MODIS) (Roy *et al.* 2008; Van Leeuwen 2008; Veraverbeke *et al.* 2014) and moderate-resolution sensors, such as Landsat (Bastarrika *et al.* 2014; Boschetti *et al.* 2015; Hawbaker *et al.* 2017). However, with the increased collection and availability of high-resolution imagery (e.g. QuickBird-2, Worldview-2, Worldview-3, GeoEye-1, RapidEye), these sources are also starting to be used to map fire events either alone (Mitri and Gitas 2006, 2008; Holden *et al.* 2010; Dragozi *et al.* 2014, 2016) or paired with Landsat imagery (Chen *et al.* 2015; Wu *et al.* 2015).

The resolution at which fires are mapped and monitored can be expected to influence our detection of within-fire heterogeneity (Lentile *et al.* 2006; Stroppiana *et al.* 2012). Heterogeneity in fire effects is common across a fire and can influence the post-fire successional trajectory and rate of vegetation recovery (Picket and White 1985; Turner *et al.* 1999). However, very few studies have used high-resolution imagery as the primary means to map fire effects, despite its finer resolution and potential to provide additional detail that could be useful in monitoring and managing burned areas. Examples of efforts to do so include studies that have, (1) related field-based burn severity to high-resolution imagery (Holden *et al.* 2010; Dragozi *et al.* 2016); (2) used high-resolution imagery to distinguish areas burned by surface and crown fires (Mitri and Gitas 2013); and (3) applied an object-based approach to map burn extent with high-resolution imagery (Dragozi *et al.* 2014).

A wide range of algorithms and techniques have been employed to map burned-area extent and severity. Most commonly, approaches rely on a reduction in visible and near-infrared surface reflectance (NIR, 0.4–1.3 μm) associated with charring and vegetation mortality (Trigg and Flasse 2000) and a rise in short wave infrared (SWIR) reflectance (1.6–2.5 μm) associated with increased soil exposure, absorption by charred

vegetation and reduction in evapotranspiration (Trigg and Flasse 2000; Smith and Hudak 2005). To account for these changes, the Normalised Burn Ratio (NBR) (Key and Benson 2006) and Normalised Difference Vegetation Index (NDVI) (Tucker 1979) are two indices commonly utilised to map burned-area extent and evaluate fire severity (Lentile *et al.* 2006), as well as monitor post-fire vegetation recovery (Goetz *et al.* 2005; Chu and Guo 2013; Soulard *et al.* 2016). Current high-resolution satellites, however, do not typically provide a SWIR band, which is required for common indices such as NBR. Correspondingly, NDVI, which relies on the red and near-infrared bands, has been commonly used to map fire dynamics and recovery with high-resolution imagery (Mitri and Gitas 2010, 2013). More recently, object-based approaches to image processing that consider not only spectral data but also object size, shape and texture in relation to other objects in the image have shown strong potential for mapping burned-area extent (Dragozi *et al.* 2014; Lohberger *et al.* 2017). Object-based approaches could also be used to classify post-fire recovery, but are only starting to be developed (Mitri and Gitas 2013; Martín-Alcón and Coll 2016).

In the present study, we explored the role that high-resolution imagery could serve in monitoring a fire event, using the Waldo Canyon fire, which occurred near the city of Colorado Springs, Colorado, USA, in 2012 as a case-study example. As the fire occurred across both a coniferous forest and scrub-shrub habitat, the case study is relevant to monitoring burned areas in both ecosystem types globally. Because of the extensive tree mortality and steep slopes, to date efforts to assess and monitor the recovery following the Waldo Canyon fire by public agencies and non-profit groups have focussed on the effects of the fire on water and soil dynamics (e.g. soil erosion, debris flows, landslides and stream flow) (Rosgen *et al.* 2013; Johnson *et al.* 2014; Dennis *et al.* 2015). However, in moderate-to-severe fire events, groundcover (e.g. vegetation, litter, mulch) has been consistently found to be the most significant factor to reduce hillslope erosion (Wagenbrenner *et al.* 2006; Larsen *et al.* 2009) and can be observed using remotely sensed imagery. Limited availability of time series of high-resolution images has restricted their use for monitoring fire effects. However, because several high-resolution images have been collected both before and following the Waldo Canyon fire, a unique opportunity presented itself to explore how high-resolution imagery can improve our ability to remotely characterise burned-area extent, severity and the recovery of vegetation following the fire. Our research questions included:

1. How does heterogeneity in burned-area extent and severity vary with image resolution?
2. How do post-fire recovery rates vary among vegetation types, as mapped by high-resolution images?

Methods

Study area

The Waldo Canyon fire was a human-caused fire within the Rampart Range, immediately north-west of the city of Colorado Springs, in El Paso County, Colorado, USA. Fire size was reported as ~7400 ha by the US Forest Service's Burned Area Emergency Response (BAER) team. Elevation within the burn perimeter ranged from 1979 to 2953 m. The fire began on 23 June 2012, and was 100% contained by 10 July 2012 (USFS 2012). It occurred on both public and private land with ~80% occurring on land owned by the US Forest Service. Landslides, debris flows and hillslope erosion were an immediate concern because of the severity of the fire and steep slopes. Slopes within the burn perimeter ranged from 0 to 64° with a mean slope of 19°. Following the fire, the BAER team applied aerial applications of agricultural straw mulch to 437 ha and woodshred mulch to 792 ha to help reduce hillslope erosion (USFS 2012). In-stream and hillslope stabilisation activities occurred across the burn extent from the summer of 2012 and have continued to present, led by a diverse range of public and non-profit groups including the US Forest Service, Colorado Springs Utility, City of Colorado Springs, Rocky Mountain Field Institute and the Coalition for the Upper South Platte. Pre-fire, the site was dominated by Douglas-fir (*Pseudotsuga menziesii*), ponderosa pine (*Pinus ponderosa*) and limber pine (*P. flexilis*), with Gambel oak (*Quercus gambelii*) dominating the lower foothills (Fig. 1). Prolific resprouting of Gambel oak following the fire allowed for a rapid recovery in the lower elevations. In the higher elevations, quaking aspen (*Populus tremuloides*) were well established by 2015, and were prolific throughout with an understorey of grasses and mullein (*Verbascum thapsus*). Species present post-fire were identified through communications with personnel familiar with the burned area as well as field visits that occurred on 25 and 26 October 2017.

Pixel-based burn area classification

High-resolution images (DigitalGlobe, Westminster, CO, USA) (GeoEye-1, QuickBird-2 and Worldview-2) were collected both before the fire and yearly following the fire (Fig. 1). Details regarding differences in the satellite characteristics are shown in Table 1, and a complete list of images utilised in the analysis are shown in Table 2. Images were acquired at 2-m resolution and processing Level 1, which allowed us to manually orthorectify each of the images. Images were orthorectified using PCI Geomatica's Optical Satellite Modelling with the Rational Function (RPC Model). A 2015 National Agricultural Imagery Program (NAIP) image (1-m resolution) was used as the reference image with the US Geological Survey's (USGS) 10-m National Elevation Dataset (NED) (Gesch *et al.* 2002). The images were converted from top-of-atmosphere to ground reflectance using ATCOR, PCI Geomatica's Atmospheric Correction module (Richter and Schläpfer 2016). Each 2012 GeoEye-1 and Worldview-2 image was processed into burned-area extent using a supervised maximum-likelihood classification. Training polygons were selected to represent (1) charred surfaces with high-conifer density and high-conifer mortality, (2) charred surfaces where pre-fire vegetation was dominated by shrubs, bare soil or low density conifers, and (3) high-conifer density where the signal was dominated by needles killed but not consumed. Each of these burned classes was classified separately, because of the distinct spectral signal and then merged post-classification. Each training polygon (two per category, six total) averaged 1 ha in size. Training polygons for category 3 were

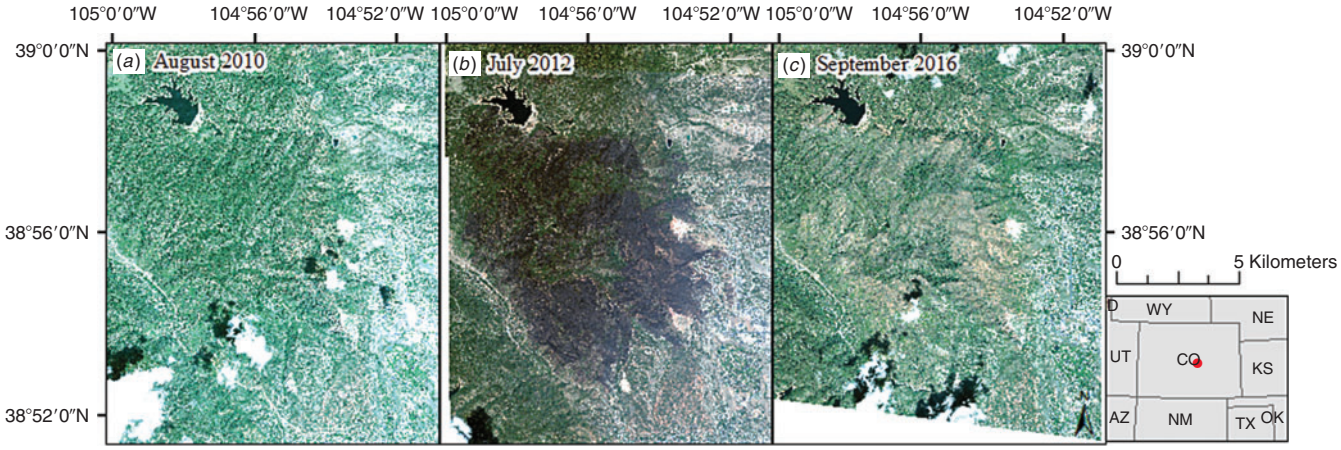

Fig. 1. Raw imagery of the study site including, (*a*) a pre-fire Worldview-2 image collected on 7 August 2010, (*b*) a Worldview-2 image collected on 4 July 2012 as the fire event was ending, and (*c*) a Worldview-3 image collected on 17 September 2016, 4 years post-fire. Copyright 2017 DigitalGlobe, NextView Licence.

Table 1. Characteristics of satellites that collected imagery over the Waldo Canyon fire burned area
Landsat ETM+, Landsat Enhanced Thematic Mapper Plus

Platform	Data availability (years)	Spatial resolution (m)	Data collection type	Image extent (km)	Spectral range (μm)	Spectral resolution (number of bands)	Sponsor, country
QuickBird-2	2001–2014	2.4 (delivered as 2 m)	On-demand	18	0.43–0.92	4	DigitalGlobe, USA
GeoEye-1	2008–present	1.65 (delivered as 2 m)	On-demand	15	0.45–0.92	4	DigitalGlobe, USA
Worldview-2	2009–present	1. 8 (delivered as 2 m)	On-demand	16	0.4–1.04	8	DigitalGlobe, USA
Worldview-3	2014–present	1.2 (delivered as 2 m)	On-demand	13	0.4–2.37	16	DigitalGlobe, USA
Landsat ETM+	1999–2003, 2003–present (scan-line corrector off)	30	Continuous (16-day revisit)	185	0.45–2.35, 10.4–12.5	8	NASA, USA

Table 2. Images used to map burned-area extent and map vegetation recovery and image date in relation to the timing of the Waldo Canyon fire which burned from June 23, 2012 to July 10, 2012
BAECV, Burned Area Essential Climate Variable; MTBS, Monitoring Trends in Burn Severity; BAER, Burned Area Emergency Response

Platform	Spatial resolution (m)	Date	Date relative to fire (July 10, 2012)
Worldview-2	2	7-Aug-10	−2 years
Worldview-2	2	7-Aug-11	−1 year
Worldview-2	2	4-Jul-12	−6 days
GeoEye-1	2	11-Jul-12	+1 day
QuickBird-2	2	25-Sept-13	1 year, 8 days
Worldview-2	2	30-Aug-14	2 years, 50 days
Worldview-3	2	30-Aug-15	3 years, 50 days
Worldview-3	2	17-Sep-16	4 years, 68 days
Landsat BAECV	30	2012 annual – compiled, 13-Jul-12 (primary image)	+ 3 days
Landsat MTBS	30	18-Sep-10 (pre), 26-Sep-13 (post)	+ 1 year, 62 days
Landsat BAER	30	11-Jun-12 (pre), 13-Jul-12 (post)	+ 3 days

smaller (~0.25 ha) as this category typically occurred in narrow bands along the edge of areas in category 1. Approximately 12 000 training pixels were used in total. Following classification, each of the burned area outputs were filtered using a 3 × 3 pixel filter. Classified results were manually edited as needed. Each version of the burned-area extent was converted to a Euclidean distance map indicating the distance to the nearest unburned pixel. Conifer seedling density following high severity wildfire has been shown to be directly related to distance from surviving forest (Donato *et al.* 2009; Kemp *et al.* 2016) and can decrease sharply as short as 50 m from the surviving forest (Chambers *et al.* 2016).

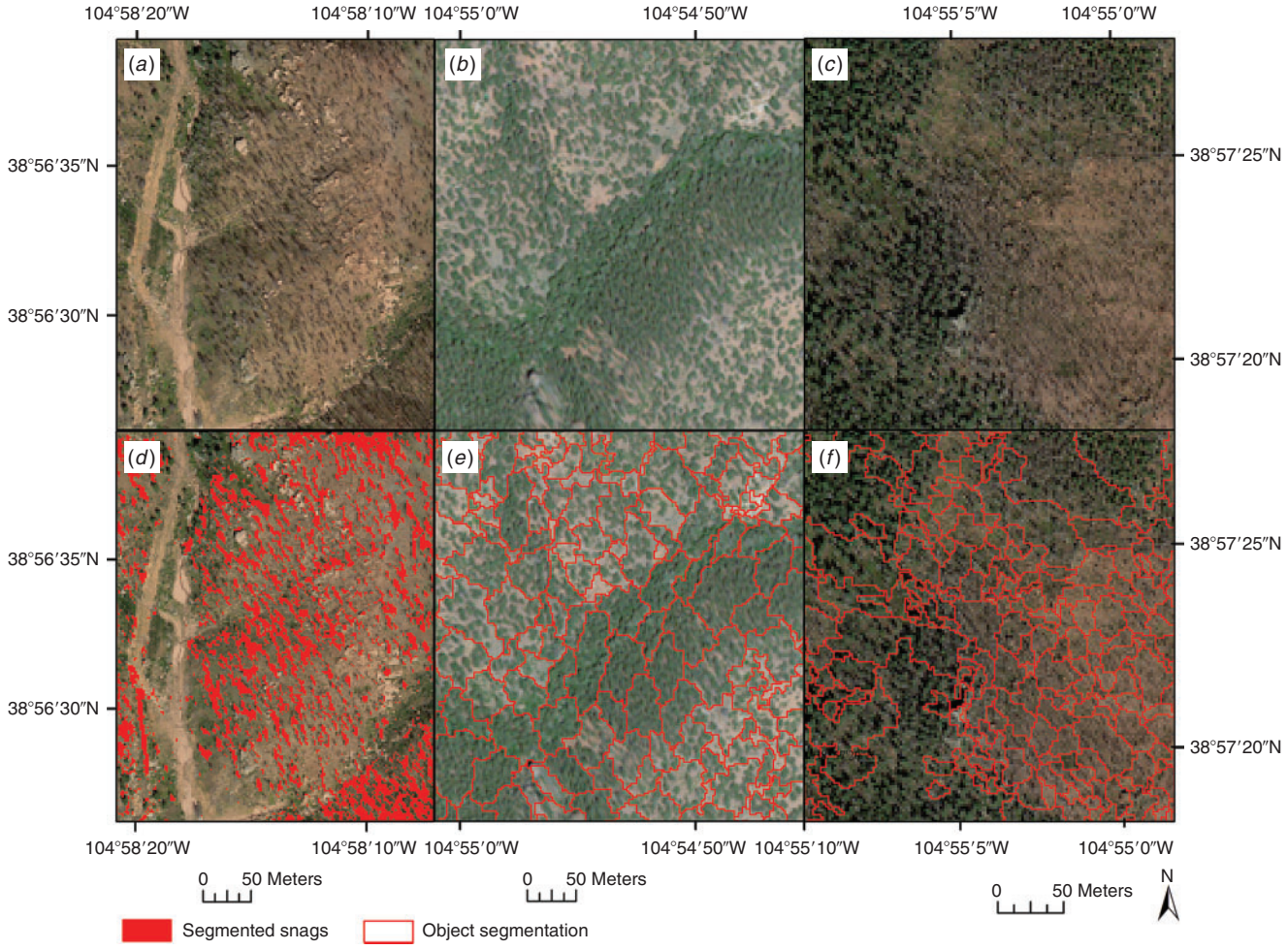

Fig. 2. High-resolution images can be segmented into individual objects such as snags (*a* and *d*, Worldview-3, from 30 August 2015) or larger objects to classify cover types from pre-fire imagery (*b* and *e*, Worldview 2, from 7 August 2011) and post-fire imagery (*c* and *f*, Worldview-3, from 30 August 2015). Copyright 2011, 2015 DigitalGlobe, NextView Licence.

Object-based burn severity

Fire-severity maps help characterise immediate and long-term fire effects (Robichaud *et al.* 2007). In using the term 'fire severity,' we are referring to a relative measure of vegetation consumption, mortality and soil alteration (e.g. charring) resulting from the fire event and measured using a relative change in surface reflectance (Lentile *et al.* 2006). We used the software, eCognition (ver. 9.2.1, Trimble, Westminster, CO, USA), to process a Worldview-2 image (collected on 4 July 2012) into burn-severity classes. This software uses an object-orientated approach in which an image is first segmented from pixels into meaningful objects or polygons, and then classified using rulesets and algorithms. The objects can represent individual trees or snags, or represent land-cover patches (Fig. 2). The 2012 Worldview-2 image was segmented into objects representing land cover patches using all bands from both the pre-fire 2011 Worldview-2 image (collected 7 August 2011) and the post-fire 2012 Worldview-2 image (collected 4 July 2012) at default segmentation levels (scale = 10, shape = 0.1, compactness = 0.5), where scale refers to the size of the objects, shape refers to the textural homogeneity of the objects (smoothness and compactness) and compactness informs the shape of the objects. The 2012 Worldview-2 image bands were assigned twice the weight of the 2011 Worldview-2 image bands to emphasise segmentation along burn severity boundaries. The 2011 image was included because burn severity depends in part on pre-fire vegetation. We used the distribution of change between the 2011 and 2012 Burned Area Index (BAI, $1 \div ((0.1 - \text{red})^2 + (0.06 - \text{NIR})^2)$) (Martin 1998) and the Soil-Adjusted Vegetation Index (SAVI, $((\text{NIR} - \text{red}) \div (\text{NIR} + \text{red} + 0.5)) \times 1.5$) (Huete 1988) for a visually identified sample of polygons or objects representing the different severity classes to develop a series of thresholds or rulesets to classify the objects into the three severity classes. SAVI was found to be more effective than NDVI because of bright soils present across parts of the site. The visually identified samples were selected by viewing the objects in relation to the pan-sharpened Worldview images (0.5-m resolution). The identification of low burn-severity samples, in particular, was also based on areas identified as such, and location recorded using a Trimble R2 GPS unit (Sunnyvale, CA,

USA) during visits to the burned area on 25 and 26 October 2017. The burn-severity categories were defined based on changes to vegetation and surface organic matter (e.g. modified from Keeley 2009):

- High severity – surface organic matter was heavily charred and canopy trees (if previously present) were killed and needles consumed.
- Moderate-severity – surface organic matter was charred. Most needles were killed but not consumed.
- Low-severity – canopy trees retained green needles, but surface indicated a faint charcoal signal.
- Unburned – no visual evidence of a burn.

Additional rulesets were developed to account for inconsistencies in the BAI or SAVI values from 2011 or 2012 for specific portions within the study area. Remaining objects that were left unclassified were segmented into smaller, more spectrally homogenous objects (scale = 5 to 7), with the classification process and the creation of rule sets repeated each time. The output was also visually checked and manually edited, as needed, in ArcGIS 10.3 (ESRI, Redlands, CA, USA). As the output was not validated against field efforts, we can only compare the distribution of severity classes relative to other severity estimates (e.g. Monitoring Trends in Burn Severity (MTBS), BAER).

Ancillary burn extent and severity datasets

Burned extent classified from GeoEye-1 and Worldview-2 was compared with burn extent produced by the USGS Landsat Burned Area Essential Climate Variable (BAECV) product, the MTBS dataset and fire statistics reported by the US Forest Services' BAER team. The BAECV product uses the entire Landsat archive to produce an annual burned-area raster for the conterminous United States (1984–2015) (Hawbaker *et al.* 2017). Its algorithm relies on a suite of predictor variables calculated from dense time series of Landsat data including both single-scene, pre-fire surface conditions (e.g. 3-year lagged means and standard deviations) and change from pre-fire surface conditions. These variables were used as the inputs to train a generalised boosted regression model (Hastie *et al.* 2009) to predict the probability that a pixel has burned in any given Landsat image. Burn-classification images were generated by applying thresholds and a region-growing method to the burn probability images.

The MTBS burn-severity rasters are classified for each fire using a histogram of the Landsat differenced Normalised Burn Ratio (dNBR) (pre- and post-fire images were collected on 18 September 2010 and 26 September 2013) (Eidenshink *et al.* 2007). We used the low, moderate and high burn-severity classes (Sparks *et al.* 2015) as a comparison for total burn extent and severity categorisation. The primary concern regarding the MTBS dataset is that class thresholds are fire specific and therefore not directly comparable across fires or necessarily related to objective ecological metrics (Kolden *et al.* 2015). We also considered the soil burn-severity raster generated by the BAER team (USFS 2012). BAER uses pre- and post-fire Landsat images to generate change to NBR (pre-and post-fire images were collected on 11 June 2012 and 13 July 2012). Teams dispatched to the burned site then collect field observations of ground cover and soil infiltration rates that are used to inform NBR thresholds. BAER defines low burn severity as showing intact ground cover, moderate severity as showing reduced ground cover and some loss of soil organics, and high burn severity as showing potential for increased flows leading to flooding and debris flows (Parsons *et al.* 2010).

Mapping vegetation recovery

Post-fire recovery of vegetation was classified using pixel-based NDVI as well as by classifying vegetation types using an object-based approach in eCognition. NDVI was calculated for the high-resolution time series images (2010–2016) across the burned area. NDVI values range from −1 (e.g. water) to 1 (dense, healthy green vegetation) (Tucker 1979). Moderate values tend to represent shrub and grassland cover types (0.2 to 0.3) whereas higher values represent areas with high above-ground biomass (0.6 to 0.8). A NDVI threshold of 0.3 was selected based on consultation with personnel very familiar with the burned site in the years immediately following the fire. This threshold is also consistent with values that have been previously used to define 'vegetated' (e.g. Gandhi *et al.* 2015) and was selected here to define areas that were vegetated pre-fire and revegetated following the fire event. In image processing, SAVI and NDVI were alternatively used when one index showed greater class separability relative to the other index.

To classify vegetation types across the time series, we first classified the pre-fire Worldview-2 image (7 August 2011) using nearest-neighbour classification in eCognition. This approach integrates multiresolution segmentation with a supervised classification algorithm. The image was segmented into objects meant to represent patches of vegetation (scale = 10, shape = 0.2, compactness = 0.5). Objects with a NDVI of <0.4 were re-segmented (scale = 7, shape = 0.1, compactness = 0.5) into smaller, more spectrally homogenous objects to improve the classification of unvegetated objects. Training objects ($n = 30$ for each class) were identified for coniferous, riparian, bare soil (i.e. bare soil, rock and sediment runoff), low-density shrub and high-density shrub cover classes. Training objects were classified and analysed using the 'Feature Space Optimisation' tool to identify the object features with the best class separation values. The object features were characterised using the following Worldview-2 band or band combinations: mean red edge band, the NIR2 band, standard deviation of green band, red edge band, NIR1 band, NIR2 band, SAVI, pixel ratios coastal band/all bands, green band/all bands, red edge band/all bands, a shape index, brightness with a near-infrared focus (red edge + NIR1 + NIR2), and a green–red vegetation index (GRVI) (Falkowski *et al.* 2005). The nearest-neighbour classification, a supervised classification, was then run for all objects within the study area. Additional rulesets were applied using elevation from the USGS NED (10-m resolution) (Gesch *et al.* 2002) and object intersection or lack of intersection with a stream as mapped by the high-resolution National Hydrography Dataset (NHD) (US Geological Survey 2013) to reduce confusion between riparian, coniferous and shrub cover types.

For the 4 July 2012 Worldview-2 image, the objects previously identified as moderate or high burn severity, were

Table 3. Recovery of vegetation following the fire across the Waldo Canyon fire study area, defined using the fire perimeter

Vegetated areas were defined as 4 m^2 cells showing a Normalised Difference Vegetation Index (NDVI) of 0.3 or greater. Revegetation began stabilising in 2015. The estimate for 2012 burned-area extent or minimal-recovery area is derived from NDVI not the pixel-based classification of burned-area extent. For reference, the influence of image collection date on NDVI values was also calculated using non-burned reference areas and presented as how the non-burned NDVI values on the image collection date compared with the annual peak NDVI values (Aspen (percentage of annual maximum), Grass (percentage of annual maximum)). NDVI values in the bottom portion of the table are derived from Landsat 8-day NDVI products available in Google Earth Engine. Minimal recovery percentage was calculated as green to non-green transition (excluding pre-fire bare soil or low vegetation areas, which comprised 12% in 7 August 2011

Date	Minimal recovery (%)	Minimal recovery (ha)	Re-vegetated to date (ha)	Satellite	Aspen (%)	Grass (%)	Landsat date (8-day product)	Peak NDVI Landsat date (aspen)	Peak NDVI Landsat date (grass)
4-Jul-12	78.2	5798.3	0	Worldview-2	100.0	48.6	11-Jul-12	11-Jul-12	28-Aug-12
25-Sep-13	49.6	3673	2125.3	QuickBird-2	97.3	96.6	22-Sep-13	21-Aug-13	21-Aug-13
30-Aug-14	35.2	2611.5	3186.8	Worldview-2	100.0	46.9	6-Sep-14	6-Sep-14	5-Aug-14
30-Aug-15	35.3	2616.2	3182.1	Worldview-3	40.7	70.6	6-Sep-15	20-Jul-15	13-Aug-15
17-Sep-16	37.6	2785.6	3012.7	Worldview-3	95.6	69.9	13-Sep-16	11-Jul-16	11-Jul-16

reclassified as minimally recovered. Unburned and low severity burned areas were assigned the 2011 cover class type. For the post-fire images (2013–2016), we used the pre-fire vegetation type and our field-based knowledge of the site-specific recovery trajectories to assist in image classification. A hierarchical approach was used where the 2012 burn severity was defined as the top level, the 2011 classified image was defined as the mid-level, and the recovery images (2013–2016) were defined as the bottom level. This approach allowed for (1) synchronisation of object edges between levels and (2) burn severity and pre-fire cover class to inform post-fire cover class. Objects classified in 2012 as burned or minimally recovered were re-segmented and reclassified in each of the post-fire years. We used SAVI thresholds, specific to each year, to indicate vegetation recovery or a shift from minimally recovered to aspen-herbaceous, riparian or shrub (recovery threshold averaged >0.37 mean SAVI). If the SAVI mean and standard deviation of the object was above a year-specific threshold, and it was classified as coniferous in 2011 and moderate or high burn severity in 2012, then the object was reclassified as coniferous (averaged >0.56 mean SAVI and >0.14 standard deviation SAVI). For objects with low SAVI values, we used brightness thresholds to distinguish between bare soil and minimally recovered objects (mean SAVI <0.27 and brightness ≥ 20.5, reclassified as bare soil). We found applying thresholds and rulesets to the post-fire images, based on the 2012 classified image, produced improved outputs relative to classifying each post-fire image independently or classifying the post-fire images as a time series. Differences in the thresholds between years suggested that variability in image quality, timing and light conditions influenced our interpretation of recovery status and creates added challenges for time series analysis.

We visited the burned area on 25 and 26 October 2017 and used GPS units to collect polygons representing homogenous vegetation classes. Although the condition of vegetation in fall (autumn) 2017 could not be used to directly validate image outputs from previous years (2011–2016), we were able to verify the major plant species present across the study area and used the polygons to increase our confidence regarding our visual interpretation of vegetation classes. Validation points ($n = 100$ per class per year) were generated randomly and assigned a class type using visual interpretation of the raw, pan-sharpened image (0.5-m resolution). When possible, points were reused across years, with the appropriate class reassessed in each year. Cover classes (e.g. water) that contributed $<2\%$ of the study area extent were not validated. Validation points were manually moved ($<2\%$ of the validation points) when we either had no visual confidence regarding the appropriate cover class or a point occurred at the intersection of two cover classes. Point movement occurred only to ensure that the vegetation class assigned to the validation points was correct. Points were located to the extent possible to represent random locations within a single cover class. In addition to visual cues, the transition from the minimally recovered class to a time when enough seedling-saplings were present and large enough to transition to the aspen-herbaceous class was made more systematic by restricting minimally recovered points to areas with a NDVI of <0.3 and restricting aspen-herbaceous validation points to areas with a NDVI of >0.3. Confidence intervals (95%) were calculated for the estimates of the percentage cover of each of the classes using the approach outline by Olofsson *et al.* (2013).

The phenology at the time of image collection can affect our interpretation of vegetation recovery. To determine the seasonality effect of image timing, we identified a homogenous area of (1) by quaking aspen (2.5 ha, 0.6 km north of burned area), and (2) grass (26 ha, 3.1 km north-west of burned area) that were not affected by the fire event. We extracted the mean NDVI value across each of the polygons for all available Landsat dates (2010–2016) using three image collections provided by Google Earth Engine (Google, Mountain View, CA, USA): (1) Landsat 5 Thematic Mapper (TM) 8-day NDVI composite, (2) Landsat 7 8-day NDVI composite, and (3) Landsat 8 8-day NDVI composite. We provided the date of the peak NDVI value in each year, as well as how the NDVI value for the Landsat date best matching the image date compared with the seasonal peak value (Table 3).

Results

Variability in the heterogeneity of burn extent and severity

Image characteristics influenced total burned-area extent. Burned-area extent tended to be smallest for our pixel-level

Table 4. Total area classified as burned, total burned area >50 m from surviving forest, and distribution of severity categories, as available, using each source of imagery

For the Worldview-2 image, the pixel-based classification results are reported for burned-area extent and object-based classification results are reported for severity distribution. BAECV, Burned Area Essential Climate Variable; MTBS, Monitoring Trends in Burn Severity; BAER, Burned Area Emergency Response

Satellite	Burned-area extent (ha)	Burned area >50 m from surviving forest (ha)	Burned area >50 m from surviving forest (%)	Low severity (%)	Moderate severity (%)	High severity (%)
GeoEye-1	5988	1840	30.7	na	na	na
Worldview-2	4387 (pixel)	598 (pixel)	13.6 (pixel)	28.8 (object)	20.0 (object)	51.2 (object)
Landsat BAECV	6495	5278	81.3	na	na	na
Landsat MTBS	7125	5669	79.6	29.6	35.9	34.5
Landsat BAER team	7385	6201	84.0	41.6	39.9	18.5

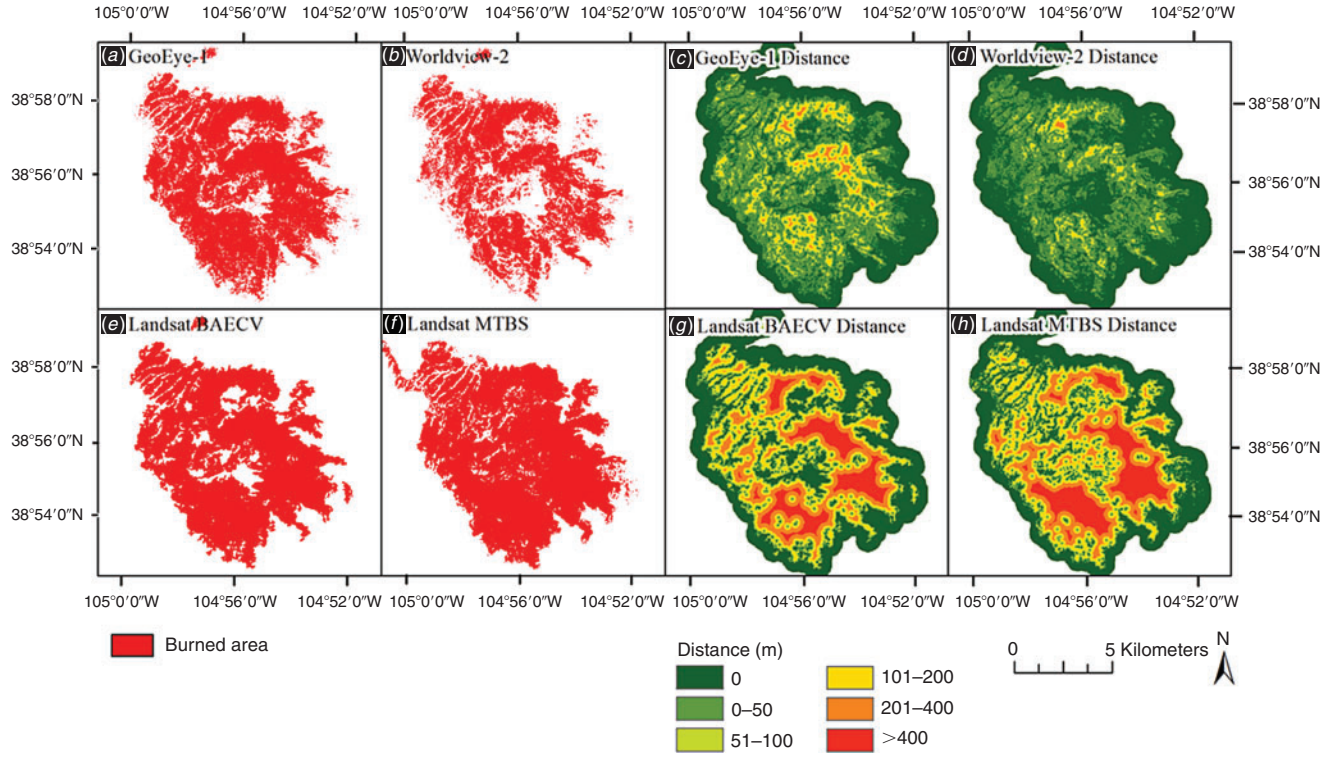

Fig. 3. Burned-area extent as mapped by (*a*) GeoEye-1 (2-m resolution), (*b*) Worldview-2 (2-m resolution), (*e*) Landsat Burned Area Essential Climate Variable (BAECV) (30-m resolution), and (*f*) Landsat Monitoring Trends in Burn Severity (MTBS) (30-m resolution), and the corresponding distance to seed sources or unburned sites (*c*, *d*, *g*, *h*).

classifications of the high-resolution imagery (5988 ha for GeoEye-1 and 4387 ha for Worldview-2) and largest for the various Landsat-based products (6495, 7385, 7125 ha for BAECV, BAER and MTBS respectively; Table 4, Fig. 3). Variability in mapped burned-area extent and within-fire heterogeneity influenced our interpretation of the amount of area at risk for reduced conifer regeneration (>50 m from surviving forest). At-risk areas ranged from 14% of the burned area mapped using Worldview-2 to 84% of the burned area mapped by the BAER team with Landsat (Table 4, Fig. 3). Fire severity as mapped using an object-based approach with a Worldview-2 image showed 51, 20 and 29% high, moderate and low burn severity respectively (Table 4, Fig. 4). In comparison, severity mapped by the MTBS dataset (an extended assessment with the post-fire image 1 year and 2 months following the fire) and the BAER team (post-fire image immediately following fire) showed greater areas identified as low and moderate severity categories, relative to the Worldview-2 output (Table 4, Fig. 4). Visually, relative to the Worldview-2 output, both BAER and MTBS overestimated low and moderate burn severity and underestimated high burn severity (Fig. 4). We note, however, that because of differences in image dates used and approaches to define severity, these differences serve primarily to highlight how variable our interpretations of burn severity can be.

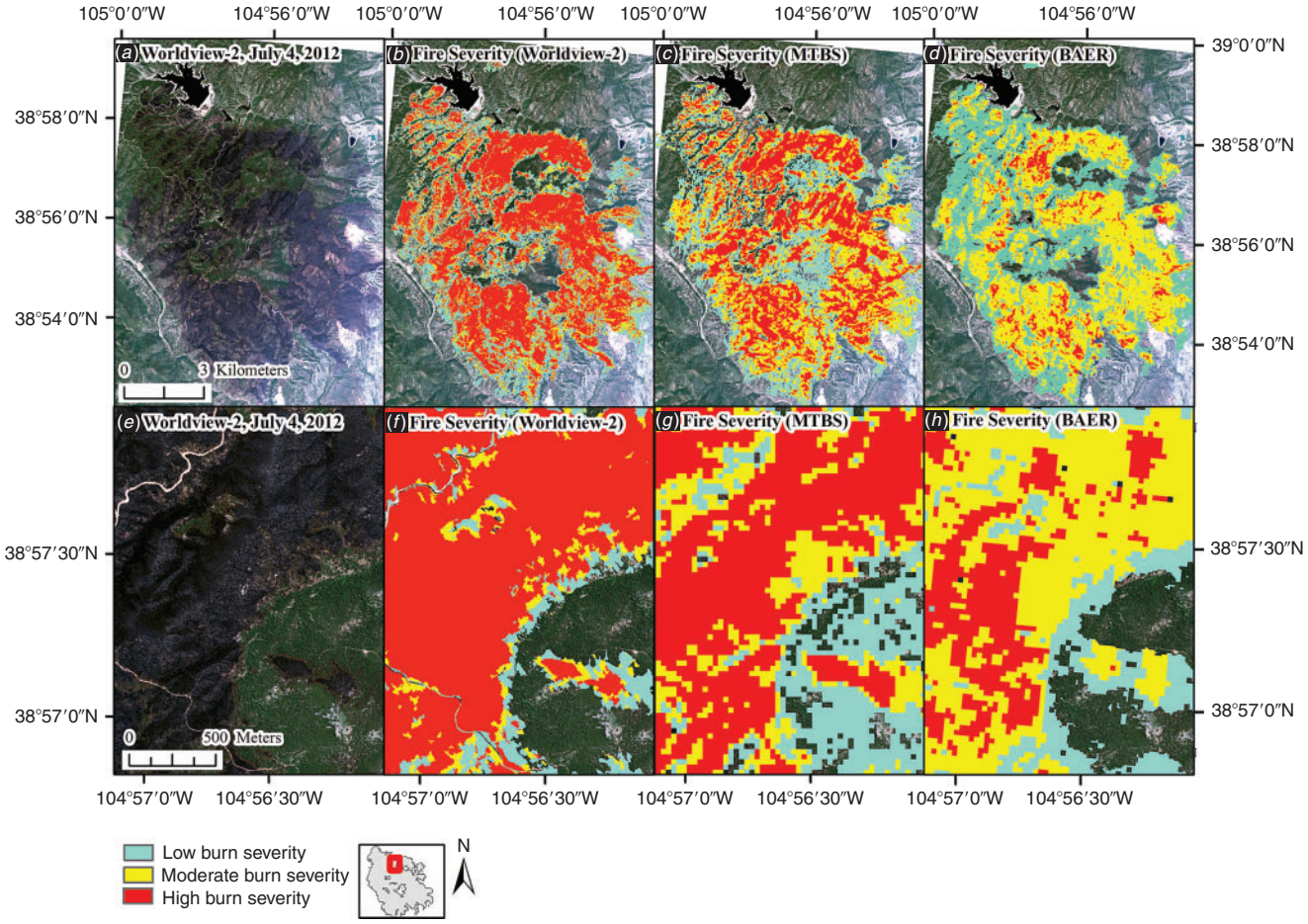

Fig. 4. (*a*) The raw image of the entire Waldo Canyon fire, a portion of the burned areas (*e*) and a comparison of mapped fire severity using Worldview-2, in eCognition (*b* and *f*) relative to the Landsat based Monitoring Trends in Burn Severity (MTBS) dataset (*c* and *g*), and the Burned Area Emergency Response (BAER) soil burn severity dataset (*d* and *h*). Copyright 2012 DigitalGlobe, NextView Licence.

Post-fire recovery across vegetation types

Using NDVI to isolate areas that showed a transition from vegetated to non-vegetated, we found that 78% of the area within the burn perimeter experienced a decline in NDVI from >0.3 to <0.3 in 2012 (Fig. 5). One year post-fire, this decreased to 50% and, by two years post-fire, this declined to 35% after which the trend stabilised (Table 3, Fig. 5). The time series of images were segmented into objects representing land cover units (Fig. 2) and then classified (Fig. 6). Overall accuracy of the cover-class maps ranged from 84 to 91% and averaged 87% for 2011–2016 (Table 5). Aspen-herbaceous showed the weakest accuracy with errors of omission and commission averaging 22 and 24% respectively. The remaining cover classes showed errors of omission (averaged) ranging from 11 to 14% and errors of commission (averaged) ranging from 2 to 17% (Table 5). Pre-fire, the study area was 73% coniferous and 19% shrub (Table 6, Fig. 6). In 2012, 62% of the study area changed to minimal recovery, whereas coniferous cover decreased to 25% and shrub to 8%. The shrub cover class recovered rapidly, within 1 year it was back to 18% (Table 6, Fig. 6). In contrast, areas that were coniferous forest have seen minimal recovery. Four years post-fire, the previously coniferous areas are divided between aspen-herbaceous (26%) and minimally recovered (22%). Riparian and bare soil cover classes, however, showed limited change in percentage cover from pre- through post-fire (Table 6). Additional examples of the classified objects both pre- and post-fire are shown in Fig. 7 and provide examples of the distribution of areas classified as minimal recovery. In addition, a line graph showing the change in vegetation cover classes from 2011 through 2016 provides a visual of the relative change in vegetation class abundance (Fig. 8).

We also compared our interpretation of vegetation cover using the pixel-based NDVI to the object-based vegetation cover classes. Because pixels showing minimal vegetation can be associated with nearby vegetated pixels when using an object-based approach, we found that the site was interpreted as showing greater vegetation cover using an object-based approach relative to using a pixel-based approach. Pre-fire, the object-based approach showed the site to be 96% vegetated, relative to the pixel-based approach that indicated 88% of the site was vegetated (Table 6). The contrast was even greater post-fire. In 2016, the object-based approach estimated that 74% of the site was vegetated, relative to 57% estimated using the pixel-based approach (Table 6).

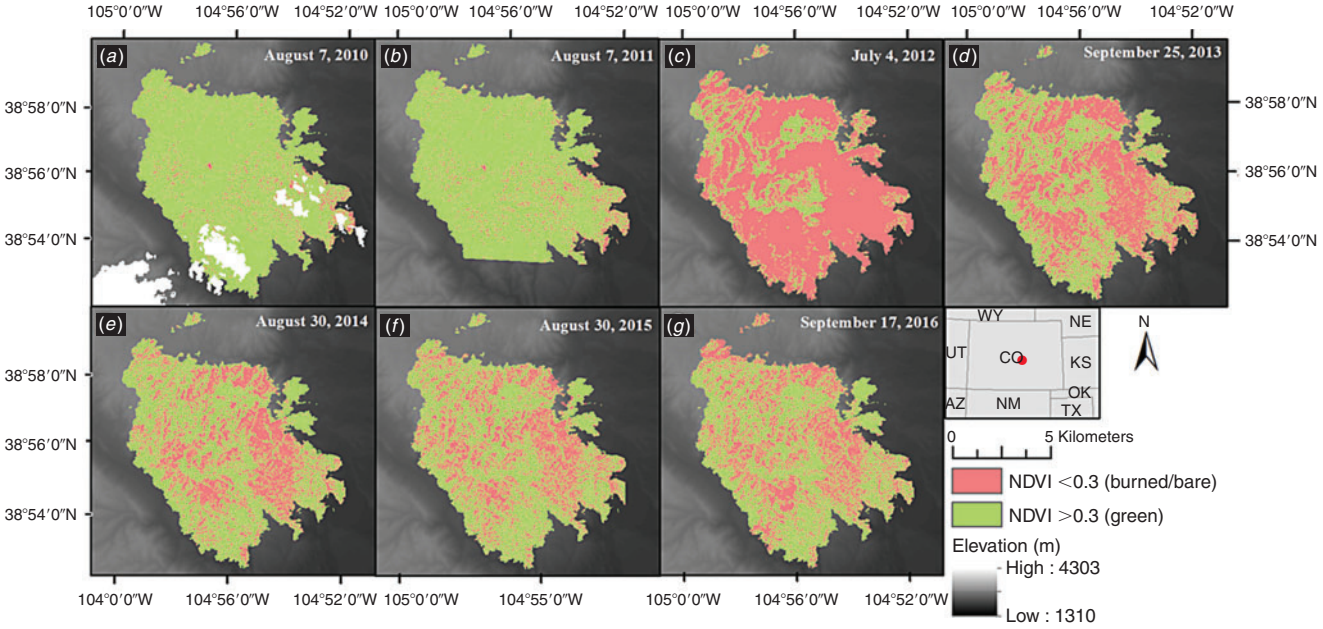

Fig. 5. Change in threshold Normalised Difference Vegetation Index (NDVI) as derived from the time series of high-resolution images from pre-fire through 4 years post-fire within the Waldo Canyon fire perimeter. Vegetated is defined as a pixel having a NDVI greater than 0.3.

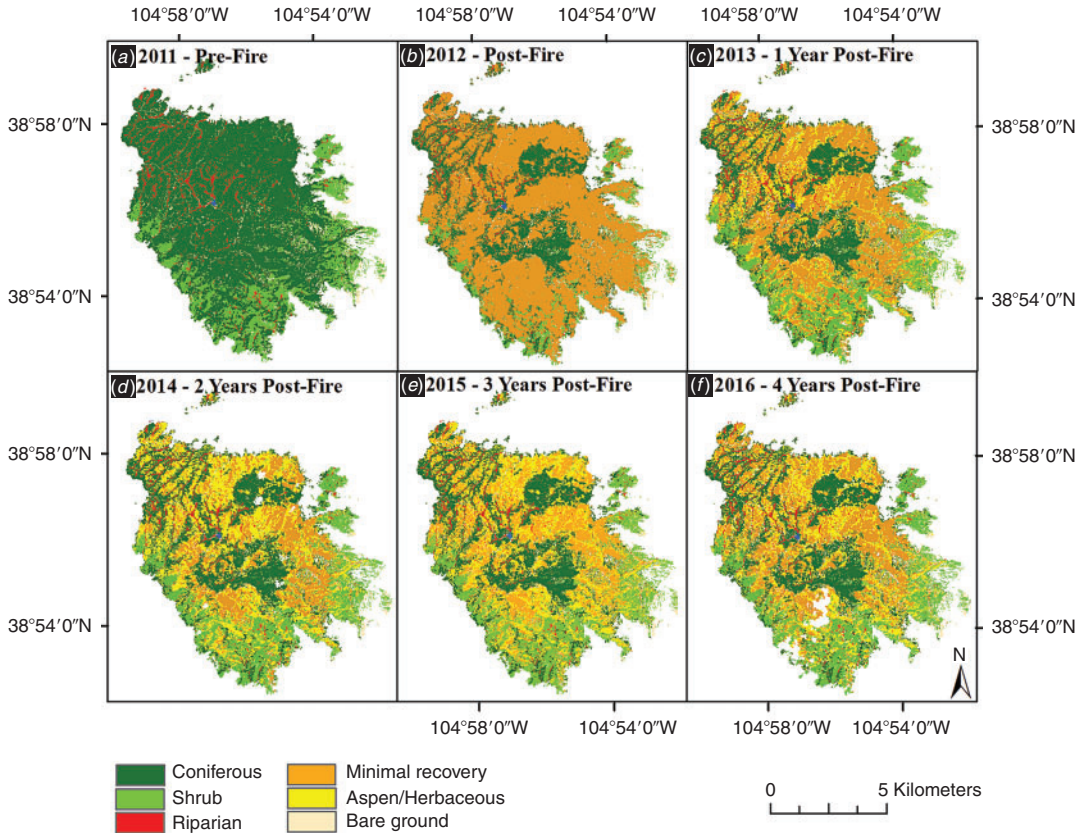

Fig. 6. Change in landcover types from pre-fire through 4 years post-fire using an object-based approach with Worldview-2 (*a*, *b*, *d*), QuickBird-2 (*c*), and Worldview-3 imagery (*e*, *f*).

Table 5. Accuracy of land cover maps by year and land cover category

Errors of omission and commission by image year and land cover category. Overall accuracy statistics are provided for each image year. Average (2011–2016) accuracy for all land cover categories as well as for each land cover category is shown in bold. NA values are listed when no areas were classified as that land cover category

Year	Overall accuracy (%)	Error type (%)	Coniferous	Riparian	Shrub	Bare ground	Minimal recovery	Aspen-herbaceous
2011	91.0	Omission	4.0	14.0	15.0	3.0	na	na
		Commission	13.5	7.5	14.1	0.0	na	na
2012	88.2	Omission	14.0	23.0	10.0	8.0	8.0	na
		Commission	20.4	8.3	17.4	0.0	11.1	na
2013	86.5	Omission	17.0	6.0	13.0	13.0	11.0	21.0
		Commission	9.8	7.8	20.2	2.2	17.6	21.0
2014	84.8	Omission	12.0	12.0	15.0	18.0	18.0	16.0
		Commission	12.9	10.2	16.7	1.2	18.8	27.0
2015	86.0	Omission	8.0	12.0	16.0	15.0	11.0	22.0
		Commission	16.4	9.3	16.0	3.4	17.6	19.6
2016	84.3	Omission	12.0	13.0	14.0	9.0	16.0	30.0
		Commission	17.0	7.4	18.1	3.2	20.8	26.3
Average	**86.8**	**Omission**	**11.2**	**13.3**	**13.8**	**11.0**	**12.8**	**22.3**
		Commission	**15.0**	**8.4**	**17.1**	**1.7**	**17.2**	**23.5**

Table 6. Relative distribution of cover classes by year (2011–2016) within the study area

Object-based recovery was defined as the percentage of the study area classified as any cover class except minimal recovery. Pixel-based recovery was defined as the percentage of the study area with a Normalised Difference Vegetation Index (NDVI) of >0.3. Cloud and cloud shadow was not included in the relative percentage and represented <1% in all years except 2016 (2.4% of the study area). 95% confidence intervals are provided for each of the cover categories for which accuracy statistics had been calculated

Year	Coniferous (%)	Riparian (%)	Shrub (%)	Bare soil (%)	Minimal recovery (%)	Aspen-herbaceous (%)	Object-based vegetated (%)	Pixel-based vegetated (%)
2011	73.2 ± 4.1	3.8 ± 1.2	18.9 ± 1.8	4.1 ± 0.5	na	na	95.9	88
2012	24.8 ± 2.2	2.1 ± 1.5	8.0 ± 1.4	3.2 ± 0.8	61.8 ± 3.6	na	34.9	19.2
2013	26.7 ± 2.1	3.6 ± 1.0	17.6 ± 1.8	3.2 ± 1.1	34.9 ± 2.6	13.9 ± 1.9	61.8	44.4
2014	26.6 ± 2.0	3.7 ± 1.3	18.3 ± 1.8	3.4 ± 1.2	16.5 ± 1.9	31.5 ± 2.8	80.1	57
2015	26.9 ± 2.0	3.7 ± 1.2	17.6 ± 1.8	3.5 ± 1.2	20.7 ± 1.8	27.6 ± 2.5	75.8	56.9
2016	26.4 ± 2.1	3.8 ± 1.2	17.8 ± 1.8	3.8 ± 0.9	22.2 ± 2.1	26.0 ± 2.7	74	54.9

Discussion

The post-fire patterns in vegetation recovery observed across the Waldo Canyon fire were consistent with expectations. Much of the area that was dominated by conifer species before the fire, transitioned to quaking aspen, a common post-fire early successional species (Fraser *et al.* 2004; Paragi and Haggstrom 2007; Smith *et al.* 2011). Seral aspen stands often transition to climax conifer stands (Smith and Smith 2005; Bergen and Dronova 2007). In the shrub dominated areas, the Gambel oak recovered quickly post-fire. Although fire readily kills the aboveground portion of Gambel oak, intense resprouting typically occurs almost immediately post-fire and often causes stands of Gambel oak to become even denser than pre-fire (Jester *et al.* 2012). At 4 years post-fire, a portion of the burned area remained classified as 'minimally recovered.' These areas fit into several categories including areas (1) dominated by dense snags either limiting or masking vegetation recovery or (2) dominated by sparse vegetation, not dense enough to show spectral similarity to aspen-herbaceous objects. Degradation of soil conditions post-fire, due to erosion and increased water repellency, particularly on steep slopes, can limit resources (e.g. water, nutrients) and result in sparser vegetation (Puigdefábregas and Sánchez 1996; Turner *et al.* 2003; Larsen *et al.* 2009). Post-fire vegetation recovery maps can potentially be used to identify such areas to inform and evaluate management decisions.

High-resolution imagery, and in particular the application of object-based approaches with high-resolution imagery, has the potential to improve our efforts to monitor post-fire recovery. Object-based approaches are most easily applied in anthropogenic settings in which features, such as roads or houses, tend to be reasonably uniform in size or shape, lending themselves to automated extraction (Lang and Blaschke 2003). In recent years, however, an increasing number of efforts have applied an object-based approach in natural settings, including post-fire environments (Mitsopoulos *et al.* 2016; Sertel and Alganci 2016; Lohberger *et al.* 2017). Using a pixel-based approach at 2-m resolution, heterogeneity present within a given cover type (e.g. scattered shrubs with a grass understorey) can complicate classification efforts. Such detailed information can make it

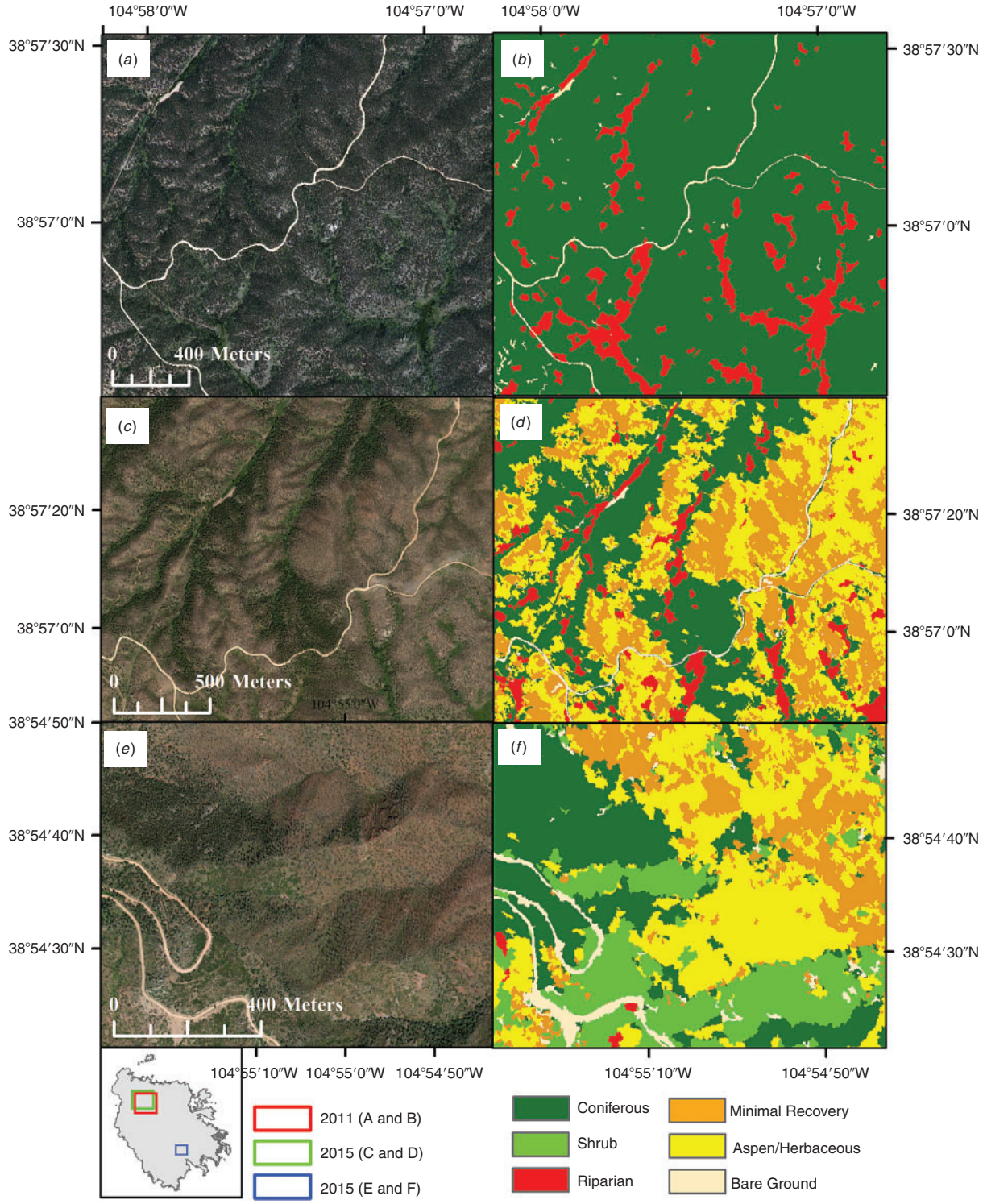

Fig. 7. Detailed examples of object-based cover classification from pre-fire conditions (*a* and *b*, Worldview-2, 7 August 2011), and post-fire conditions (*c* and *d*, *e* and *f*, Worldview-3, from 30 August 2015). Copyright 2011, 2015 DigitalGlobe, NextView Licence.

challenging to classify both grass and shrub pixels as a shrub-cover type. Object-based approaches can improve such efforts (e.g. Laliberte *et al.* 2004), but natural diversity across a single cover class (e.g. wetland grasses *v.* willows in a riparian habitat, varying shrub or conifer density) can also make it challenging to obtain adequate accuracy. The advantage of an object-based approach is that it pairs common classifications (e.g. supervised classification, random forest) with additional decision points

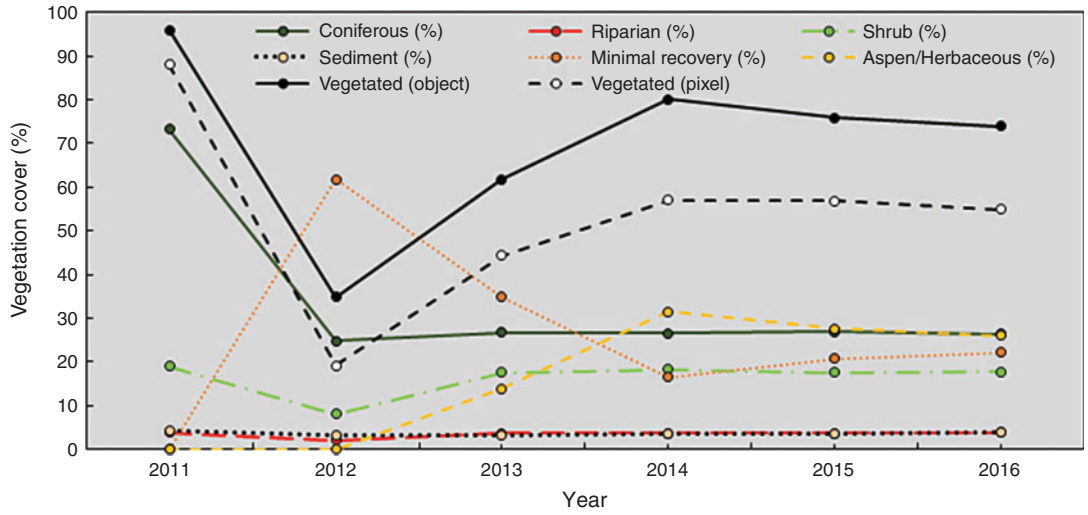

Fig. 8. The percentage cover of each vegetation class from 2011 to 2016 across the burned-area extent, as classified by the eCognition outputs. The total percentage of the burned area classified as vegetated using the object-based approach and Normalised Difference Vegetation Index (NDVI) thresholded pixel-based approach is also shown.

including object creation, applying a hierarchical structure to input datasets, and the option to implement additional rulesets and thresholds before classification. This flexibility allows users to enhance outputs, but alternatively, classification efforts can rapidly become time intensive and an algorithm personalised to a specific site makes it challenging to automate the approach at a larger scale or transfer the approach to other sites.

The application of high-resolution imagery to burned areas can enable the mapping of live crowns and small patches of bare soil (<100 m^2), rock and unburned vegetation within an otherwise continuous burned area (Vanderhoof *et al.* 2017). How these detailed features are mapped will, in turn, influence estimates of burned area and fire effects. For example, recent studies have documented the effect of distance to unburned areas on conifer regeneration (Donato *et al.* 2009; Chambers *et al.* 2016; Kemp *et al.* 2016). The present study demonstrated how our interpretation of distance to unburned changes, and consequently, our interpretation of conifer regeneration probability, when using high-resolution imagery relative to Landsat imagery.

However, spatial resolution is not the only driver of burned-area extent. Total-burned area also varied between the two sources of high-resolution imagery despite identical spatial resolutions and similar spectral ranges. Differences can be attributed to variability in image quality and timing of image collection. In this case, the Worldview-2 image was collected 6 days before the fire being extinguished. Differences can also be attributed to image classification techniques, which may explain the differences in burned-area extent as defined by the BAECV, MTBS and BAER efforts, all of which relied on Landsat imagery. Differences between the Landsat burned area and high-resolution burned area is likely attributable to multiple of these factors. For example the BAECV algorithm contained a region-growing component (Hawbaker *et al.* 2017) that likely reduced within-fire heterogeneity, whereas the resolution of the high-resolution DigitalGlobe imagery was more conducive to identifying within-fire heterogeneity.

Consistent classification of fire severity is even more challenging than mapping burned-area extent as fire severity can refer to multiple aspects of a fire event (Lentile *et al.* 2006). This is evident in Fig. 4, as very high tree mortality resulted in much of the burned area being classified as high severity by our analysis, but classified as moderate severity by the BAER team, which focussed on soil. Even if we can agree to a general definition of fire severity, for instance, referring to the loss of organic matter or changes to soil characteristics (Keeley 2009), linking remotely sensed measurements to the physical or ecological processes can be difficult (Lentile *et al.* 2006). However, remote classification of severity is essential as fire severity has implications for ecosystem recovery including shifts in species composition, soil stabilisation and carbon emissions (Kokaly *et al.* 2007; Meigs *et al.* 2009; Johnstone *et al.* 2011). Our finding that MTBS may have overestimated low burn severity and underestimated high burn severity is consistent with the findings of others (e.g. Cansler and McKenzie 2012) and represents a concern previously raised by Kolden *et al.* (2015). However in this case, MTBS mapped severity as an extended assessment, meaning that the post-fire image was collected more than 1 year post-fire and this lag may have influenced the interpretation of burn severity categories. Regardless, standardising fire severity classification methods across diverse fires and ecosystems remains a considerable challenge.

Although efforts to monitor fire events remain dominated by coarser-resolution satellites such as Landsat, AVHRR and MODIS, the launch of networks of microsatellites (e.g. Dove, RapidEye (Planet, San Francisco, CA, USA)), will provide nearly complete spatial coverage at near-daily return intervals and at a global scale, greatly improving opportunities to apply high-resolution imagery ($\leq$5-m resolution) to fire events across the globe. Differences in image resolution, extent and spectral bands, relative to Landsat, mean novel approaches may be necessary to allow for the effective application of this imagery type to map and monitor fire events.

Conclusion

In this study, we found that applying an object-based approach to a time series of high-resolution images collected both pre- and post-fire, allowed us to move beyond simplistic measures of vegetation recovery (e.g. NDVI) and assess differential rates in recovery across pre-fire vegetation classes. Output maps produced using such an approach could be used to inform management actions or evaluate the potential effectiveness of post-fire treatments. We also found that imagery source can influence interpretation of post-fire burn condition (i.e. burned-area extent, severity and heterogeneity). Variation in these parameters can, in turn, affect perceived needs for post-fire treatment across a burned area. Although these patterns should be assessed across a diversity of fires, the findings are consistent with Vanderhoof *et al.* (2017) in which fire heterogeneity was found to be closely related to image resolution. Linking remote sensing efforts to the scale at which management decisions are made (e.g. tree, patch, fire event) will be critical to informing the appropriate resolution of imagery to be used in post-fire assessments. As high-resolution, multispectral imagery becomes increasingly available, so will opportunities for remote, detailed monitoring of post-fire conditions.

Conflicts of interest

The authors declare that they have no conflicts of interest.

Acknowledgements

We thank the US Geological Survey, Climate and Land Use Mission Area, Land Remote Sensing Program for providing funding to support this research. High-resolution imagery was provided through the NextView Licence. We also thank Gordon Brenner with the City of Colorado Springs for his assistance in flying imagery and coordinating site visits as well as Miguel Villarreal and two anonymous reviewers for their insightful comments on earlier versions of the manuscript. Any use of trade, firm, or product names is for descriptive purposes only and does not imply endorsement by the USA Government. Data generated in this study will be publicly available through ScienceBase (https://doi.org/10.5066/P9NWJQJR) following publication.

References

Bastarrika A, Alvarado M, Artano K, Martinez MP, Mesanza A, Torre L, Ramo R, Chuvieco E (2014) BAMS: a tool for supervised burned area mapping using Landsat data. *Remote Sensing* **6**(12), 12360–12380. doi:10.3390/RS61212360

Bergen KM, Dronova I (2007) Observing succession on aspen-dominated landscapes using a remote sensing-ecosystem approach. *Landscape Ecology* **22**, 1395–1410. doi:10.1007/S10980-007-9119-1

Bond WJ, Woodward FI, Midgley GF (2005) The global distribution of ecosystems in a world without fire. *New Phytologist* **165**, 525–538. doi:10.1111/J.1469-8137.2004.01252.X

Bond-Lamberty B, Peckham SD, Ahl DE, Gower ST (2007) Fire as the dominant driver of central Canadian boreal forest carbon balance. *Nature* **450**, 89–92. doi:10.1038/NATURE06272

Boschetti L, Roy DP, Justice CO, Humber ML (2015) MODIS-Landsat fusion for large area 30 m burned area mapping. *Remote Sensing of Environment* **161**, 27–42. doi:10.1016/J.RSE.2015.01.022

Cansler CA, McKenzie D (2012) How robust are burn severity indices when applied in a new region? Evaluation of alternate field-based and remote-sensing methods. *Remote Sensing* **4**(2), 456–483. doi:10.3390/RS4020456

Chambers ME, Fornwalt PJ, Malone SL, Battaglia MA (2016) Patterns of conifer regeneration following high severity wildfire in ponderosa pine – dominated forests of the Colorado Front Range. *Forest Ecology and Management* **378**, 57–67. doi:10.1016/J.FORECO.2016.07.001

Chen G, Metz MR, Rizzo DM, Meentemeyer RK (2015) Mapping burn severity in a disease-impacted forest landscape using Landsat and MASTER imagery. *International Journal of Applied Earth Observation and Geoinformation* **40**, 91–99. doi:10.1016/J.JAG.2015.04.005

Chu T, Guo X (2013) Remote sensing techniques in monitoring post-fire effects and patterns of forest recovery in boreal forest regions: a review. *Remote Sensing* **6**, 470–520. doi:10.3390/RS6010470

Conard SG, Sukhinin AI, Stocks BJ, Cahoon DR, Davidenko EP, Ivanova GA (2002) Determining effects of area burned and fire severity on carbon cycling and emissions in Siberia. *Climatic Change* **55**, 197–211. doi:10.1023/A:1020207710195

Dennis MS, Joseph EG, Jason WK (2015) Objective definition of rainfall intensity-duration thresholds for post-fire flash floods and debris flows in the area burned by the Waldo Canyon Fire, Colorado, USA. In 'Engineering Geology for Society and Territory – Volume 2'. (Eds G Lollino, A Manconi, J Clague, W Shan, M Chiarle) pp. 621–624. (Springer: New York)

Donato DC, Fontain JB, Campbell JL, Robinson WD, Kauffman JB, Law BE (2009) Conifer regeneration in stand-replacement portions of a large mixed-severity wildfire in the Klamath–Siskiyou Mountains. *Canadian Journal of Forest Research* **39**(4), 823–838. doi:10.1139/X09-016

Dragozi E, Gitas IZ, Stavrakoudis DG, Theocharis JB (2014) Burned area mapping using support vector machines and the FuzCoC feature selection method on VHR IKONOS imagery. *Remote Sensing* **6**, 12005–12036. doi:10.3390/RS61212005

Dragozi E, Gitas IZ, Bajocco S, Stavrakoudis DG (2016) Exploring the relationship between burn severity field data and very high resolution GeoEye images: the case of the 2011 Evros wildfire in Greece. *Remote Sensing* **8**, 566. doi:10.3390/RS8070566

Eidenshink J, Schwind B, Brewer K, Zhu Z, Quayle B, Howard S (2007) A project for monitoring trends in burn severity. *Fire Ecology* **3**, 3–21. doi:10.4996/FIREECOLOGY.0301003

Falkowski MJ, Gessler PE, Morgan P, Hudak AT, Smith AMS (2005) Characterizing and mapping forest fire fuels using ASTER imagery and gradient modeling. *Forest Ecology and Management* **217**, 129–146. doi:10.1016/J.FORECO.2005.06.013

Fraser E, Landhausser S, Lieffer V (2004) The effect of fire severity and salvage logging traffic on regeneration and early growth of aspen suckers in north-central Alberta. *Forestry Chronicle* **80**, 251–256. doi:10.5558/TFC80251-2

Gandhi GM, Parthiban S, Thummalu N, Christy A (2015) NDVI: vegetation change detection using remote sensing and GIS – a case study of Vellore District. *Procedia Computer Science* **57**, 1199–1210. doi:10.1016/J.PROCS.2015.07.415

Gesch D, Oimoen M, Greenlee S, Nelson C, Steuck M, Tyler D (2002) The national elevation dataset. *Photogrammetric Engineering and Remote Sensing* **68**(1), 5–11.

Giglio L, Randerson JT, van der Werf GR (2013) Analysis of daily, monthly, and annual burned area using the fourth-generation global fire emissions database (GFED4). *Journal of Geophysical Research. Biogeosciences* **118**(1), 317–328. doi:10.1002/JGRG.20042

Goetz SJ, Bunn AG, Fiske GJ, Houghton RA (2005) Satellite-observed photosynthetic trends across boreal North America associated with climate and fire disturbance. *Proceedings of the National Academy of Sciences of the United States of America* **102**, 13521–13525. doi:10.1073/PNAS.0506179102

Hastie T, Tibshirani R, Friedman J (2009) 'The Elements of Statistical Learning; Data Mining, Inference, and Prediction', 2nd edn. (Springer: New York, NY, USA)

Hawbaker TJ, Vanderhoof MK, Beal Y-J, Takacs JD, Schmidt G, Falgout J, Brunner N, Caldwell M, Dwyer J (2017) An automated approach to identify burned areas in Landsat images. *Remote Sensing of Environment* **198**, 504–522. doi:10.1016/J.RSE.2017.06.027

Hayes JJ, Robeson SM (2011) Relationships between fire severity and post-fire landscape pattern following a large mixed-severity fire in the Valle Vidal, New Mexico, USA. *Forest Ecology and Management* **261**, 1392–1400. doi:10.1016/J.FORECO.2011.01.023

Holden ZA, Morgan P, Smith AMS, Vierling L (2010) Beyond Landsat: A comparison of four satellite sensors for detecting burn severity in ponderosa pine forests of the Gila Wilderness, NM, USA. *International Journal of Wildland Fire* **19**, 449–458. doi:10.1071/WF07106

Huete AR (1988) A soil-adjusted vegetation index (SAVI). *Remote Sensing of Environment* **25**(3), 295–309. doi:10.1016/0034-4257(88)90106-X

Jester N, Rogers K, Dennis FC (2012) Gambel oak management. Natural Resources Series-Forestry. Colorado State University Extension, Fact Sheet number 6.311. (Fort Collins, CO, USA)

Johnson RH, Schumacher RS, Ruppert JH, Jr, Lindsey DT, Ruthford JE, Kriederman L (2014) The role of convective outflow in the Waldo Canyon fire. *Monthly Weather Review* **142**, 3061–3080. doi:10.1175/MWR-D-13-00361.1

Johnstone JF, Rupp TS, Olson M, Verbyla D (2011) Modeling impacts of fire severity on successional trajectories and future fire behavior in Alaskan boreal forests. *Landscape Ecology* **26**(4), 487–500. doi:10.1007/S10980-011-9574-6

Keeley JE (2009) Fire intensity, fire severity and burn severity: a brief review and suggested usage. *International Journal of Wildland Fire* **18**, 116–126. doi:10.1071/WF07049

Kemp KB, Higuera PE, Morgan P (2016) Fire legacies impact conifer regeneration across environmental gradients in the US northern Rockies. *Landscape Ecology* **31**(3), 619–636. doi:10.1007/S10980-015-0268-3

Key CH, Benson NC (2006) Landscape assessment: Sampling and analysis methods. In 'FIREMON: Fire Effects Monitoring and Inventory System'. (Eds DC Lutes, RE Keane, JF Caratti, CH Key, NC Benson, and LJ Gangi) USDA Forest Service, Rocky Mountain Research Station, General Technical Report RMRS-GTR-164-CD. (Fort Collins, CO, USA)

Kokaly RF, Rockwell BW, Haire SL, King TVV (2007) Characterization of post-fire surface cover, soils, and burn severity at the Cerro Grande Fire, New Mexico, using hyperspectral and multispectral remote sensing. *Remote Sensing of Environment* **106**(3), 305–325. doi:10.1016/J.RSE.2006.08.006

Kolden CA, Smith AMS, Abatzoglou JT (2015) Limitations and utilization of Monitoring Trends in Burn Severity products for assessing wildfire severity in the USA. *International Journal of Wildland Fire* **24**, 1023–1028.

Laliberte AS, Rango A, Havstad KM, Paris JF, Beck RF, McNeely R, Gonzalez AL (2004) Object-oriented image analysis for mapping shrub encroachment from 1937 to 2003 in southern New Mexico. *Remote Sensing of Environment* **93**(1–2), 198–210. doi:10.1016/J.RSE.2004.07.011

Lang S, Blaschke T (2003) Hierarchical object representation – comparative multi-scale mapping of anthropogenic and natural features. *International Archives of Photogrammetry, Remote Sensing and Spatial Information Sciences* **34**(part 3/W8), 181–186.

Larsen IJ, MacDonald LH, Brown E, Rough D, Welsh MJ, Pietraszek JH, Libohova Z, de Dio Benavides-Solorio J, Schaffrath K (2009) Causes of post-fire runoff and erosion: water repellency, cover, or soil sealing? *Soil Science Society of America Journal* **73**(4), 1393–1407. doi:10.2136/SSSAJ2007.0432

Lentile LB, Holden ZA, Smith AMS, Falkowski MJ, Hudak AT, Morgan P, Lewis SA, Gessler PE, Benson NC (2006) Remote sensing techniques to assess active fire characteristics and post-fire effects. *International Journal of Wildland Fire* **15**, 319–345. doi:10.1071/WF05097

Lohberger S, Stangel M, Atwood EC, Siegert F (2017) Spatial evaluation of Indonesia's 2015 fire-affected area and estimated carbon emissions using Sentinel-1. *Global Change Biology*. doi:10.1111/GCB.13841

Martin MP (1998) Cartografía e inventario de incendios forestales en la Península Ibérica a partir de imágenes NOAA AVHRR. PhD thesis, Departamento de Geografia, Universidad de Alcalá, Alcalá de Henares, Madrid, Spain.

Martín-Alcón S, Coll L (2016) Unraveling the relative importance of factors driving post-fire regeneration trajectories in non-serotinous *Pinus nigra* forests. *Forest Ecology and Management* **361**, 13–22. doi:10.1016/J.FORECO.2015.11.006

Meigs GW, Donato DC, Campbell JL, Martin JG, Law BE (2009) Forest fire impacts on carbon uptake, storage, and emission: the role of burn severity in the Eastern Cascades, Oregon. *Ecosystems* **12**(8), 1246–1267. doi:10.1007/S10021-009-9285-X

Mitri GH, Gitas IZ (2006) Fire type mapping using object-based classification of Ikonos imagery. *International Journal of Wildland Fire* **15**, 457–462. doi:10.1071/WF05085

Mitri GH, Gitas IZ (2008) Mapping the severity of fire using object-based classification of IKONOS imagery. *International Journal of Wildland Fire* **17**, 431–442. doi:10.1071/WF07103

Mitri GH, Gitas IZ (2010) Mapping postfire vegetation recovery using EO-1 Hyperion imagery *IEEE Transactions on Geoscience and Remote Sensing* **48**(3), 1613–1618. doi:10.1109/TGRS.2009.2031557

Mitri GH, Gitas IZ (2013) Mapping post-fire forest regeneration and vegetation recovery using a combination of very high spatial resolution and hyperspectral satellite imagery. *International Journal of Applied Earth Observation and Geoinformation* **20**, 60–66. doi:10.1016/J.JAG.2011.09.001

Mitsopoulos I, Mallinis G, Karali A, Giannakopoulos C, Arianoutsou M (2016) Mapping fire behavior under changing climate in a Mediterranean landscape in Greece. *Regional Environmental Change* **16**(7), 1929–1940. doi:10.1007/S10113-015-0884-0

Moreno-Ruiz JA, Garcia-Lazaro JR, Riano D, Kefauver SC (2014) The synergy of the 0.05° (~5 km) AVHRR Long Term Data Record (LTDR) and Landsat TM archive to map large fires in the North American boreal region from 1984 to 1998. *IEEE Journal of Selected Topics in Applied Earth Observations Remote Sensing* **7**(4), 1157–1166. doi:10.1109/JSTARS.2013.2292853

Olofsson P, Foody GM, Stehman SV, Woodcock CE (2013) Making better use of accuracy data in land change studies: Estimating accuracy and area and quantifying uncertainty using stratified estimation. *Remote Sensing of Environment* **129**, 122–131. doi:10.1016/J.RSE.2012.10.031

Palacios-Orueta A, Chuvieco E, Parra A, Carmona-Moreno C (2005) Biomass burning emissions: a review of models using remote-sensing data. *Environmental Monitoring and Assessment* **104**, 189–209. doi:10.1007/S10661-005-1611-Y

Paragi TF, Haggstrom DA (2007) Short-term responses of aspen to fire and mechanical treatments in interior Alaska *Northern Journal of Applied Forestry* **24**(2), 153–157.

Parisien M, Peters V, Wang Y, Little J, Bosch E, Stocks B (2006) Spatial patterns of forest fires in Canada, 1980–1999. *International Journal of Wildland Fire* **15**, 361–374. doi:10.1071/WF06009

Parsons A, Robichaud PR, Lewis SA, Napper C, Clark JT (2010) Field guide for mapping post-fire soil burn severity. USDA, Forest Service, Rocky Mountain Research Station, General Technical Report RMRS-GTR-243. (Fort Collins, CO, USA) Available at https://www.fs.fed.us/rm/pubs/rmrs_gtr243.pdf [Verified 19 September 2017]

Picket ST, White PS (1985) National disturbance and patch dynamics: an introduction. In 'The Ecology of Natural Disturbance and Patch

Dynamics'. (Eds ST Picket, PS White) pp. 3–13. (Academic Press: New York, NY, USA)

Puigdefábregas J, Sánchez G (1996) Geomorphological implications of vegetation patchiness on semi-arid slopes. In 'Advances in Hillslope Processes'. (Eds MG Anderson, SM Brooks) pp. 1027–1059. (Wiley: Chichester, UK)

Randerson JT, van der Werf GR, Collatz GJ, Giglio L, Still CJ, Kasibhatla P, Miller JB, White JWC, DeFries RS, Kasischke ES (2005) Fire emissions from C_3 and C_4 vegetation and their influence on interannual variability of atmospheric CO_2 and $\delta^{13}CO_2$. *Global Biogeochemical Cycles* **19**. doi:10.1029/2004GB002366

Richter R, Schläpfer D (2016) Atmospheric/topographic correction for satellite imagery; ATCOR-2/3 user guide, version 9.0.2. (ReSe Applications: Langeggweg, Switzerland) Available at http://atcor.com/pdf/atcor3_manual.pdf [Verified 8 February 2017]

Robichaud PR, Lewis SA, Laes DYM, Hudak AT, Kokaly RF, Zamudio JA (2007) Postfire soil burn severity mapping with hyperspectral image unmixing. *Remote Sensing of Environment* **108**, 467–480. doi:10.1016/J.RSE.2006.11.027

Rosgen D, Rosgen B, Collins S, Nankervis J, Wright K (2013) Waldo Canyon Fire watershed assessment: the WARSSS results. Coalition for the Upper South Platte, Lake George, CO, USA.

Roy DP, Boschetti L, Justice CO, Ju J (2008) The collection 5 MODIS burned area product – global evaluation by comparison with the MODIS active fire product. *Remote Sensing of Environment* **112**, 3690–3707. doi:10.1016/J.RSE.2008.05.013

Sertel E, Alganci U (2016) Comparison of pixel and object-based classification for burned area mapping using SPOT-6 images. *Geomatics, Natural Hazards & Risk* **7**(4), 1198–1206. doi:10.1080/19475705.2015.1050608

Smith AMS, Hudak AT (2005) Estimating combustion of large downed woody debris from residual white ash. *International Journal of Wildland Fire* **14**, 245–248. doi:10.1071/WF05011

Smith AE, Smith FW (2005) Twenty-year change in aspen dominance in pure aspen and mixed aspen/confier stands on the Uncompahgre Plateau, Colorado USA. *Forest Ecology and Management* **213**, 338–348. doi:10.1016/J.FORECO.2005.03.018

Smith EA, O'Loughlin D, Buck JR, St. Clair SB (2011) The influences of conifer succession, physiographic conditions and herbivory on quaking aspen regeneration after fire. *Forest Ecology and Management* **262**(3), 325–330. doi:10.1016/J.FORECO.2011.03.038

Sommers WT, Loehman RA, Hardy CC (2014) Wildland fire emissions, carbon, and climate: science overview and knowledge needs. *Forest Ecology and Management* **317**, 1–8. doi:10.1016/J.FORECO.2013.12.014

Soulard CE, Albano CM, Villarreal ML, Walker JJ (2016) Continuous 1985–2012 Landsat monitoring to assess fire effects on meadows in Yosemite National Park, California. *Remote Sensing* **8**, 371. doi:10.3390/RS8050371

Sparks AM, Boschetti L, Smith AMS, Tinkham WT, Lannom KO, Newingham BA (2015) An accuracy assessment of the MTBS burned area product for shrub–steppe fires in the northern Great Basin, United States. *International Journal of Wildland Fire* **24**, 70–78. doi:10.1071/WF14131

Stroppiana D, Bordogna G, Carrara P, Boschetti M, Boschetti L, Brivio PA (2012) A method for extracting burned areas from Landsat TM/ETM+ images by soft aggregation of multiple spectral indices and a region growing algorithm. *ISPRS Journal of Photogrammetry and Remote Sensing* **69**, 88–102. doi:10.1016/J.ISPRSJPRS.2012.03.001

Trigg S, Flasse S (2000) Characterising the spectral-temporal response of burned savanna using in situ spectroradiometry and infrared thermometry. *International Journal of Remote Sensing* **21**, 3161–3168. doi:10.1080/01431160050145045

Tucker CJ (1979) Red and photographic infrared linear combinations for monitoring vegetation. *Remote Sensing of Environment* **8**, 127–150. doi:10.1016/0034-4257(79)90013-0

Turner MG, Romme WH, Garner RH (1999) Prefire heterogeneity, fire severity and early post-fire plant reestablishment in subalpine forests of Yellowstone National Park, Wyoming. *International Journal of Wildland Fire* **9**, 21–36. doi:10.1071/WF99003

Turner MG, Romme WH, Reed RA, Tuskan GA (2003) Post-fire aspen seedling recruitment across the Yellowstone (USA) landscape. *Landscape Ecology* **18**(2), 127–140. doi:10.1023/A:1024462501689

US Forest Service (2012) Waldo Canyon fire burned area emergency response (BAER) briefing. Burned-Area (BAER) Report (FS-2500–8). InciWeb, Incident Information System. Available at https://inciweb.nwcg.gov/photos/COPSF/2012-06-23-16:51-waldo-canyon-fire/related_files/ftp-20120830-190659.pdf [Verified 19 September 2017]

US Geological Survey (2013) The National Hydrography Dataset (NHD). (US Geological Survey: Reston, VA, USA) Available at ftp://nhdftp.usgs.gov/DataSets/Staged/States/FileGDB/HighResolution/ [Verified 15 December 2017]

Van Leeuwen WJD (2008) Monitoring the effects of forest restoration treatments on post-fire vegetation recovery with MODIS multitemporal data. *Sensors* **8**(3), 2017–2042. doi:10.3390/S8032017

Vanderhoof MK, Brunner NM, Beal Y-JG, Hawbaker TJ (2017) Evaluation of the USGS Landsat Burned Area Essential Climate Variable across the conterminous US using commercial high-resolution imagery. *Remote Sensing* **9**(743), 1–24.

Veraverbeke S, Sedano F, Hook SJ, Randerson JT, Jin Y, Rogers BM (2014) Mapping the daily progression of large wildland fires using MODIS active fire data. *International Journal of Wildland Fire* **23**(5), 655–667. doi:10.1071/WF13015

Wagenbrenner JW, MacDonald LH, Rough D (2006) Effectiveness of three post-fire rehabilitation treatments in the Colorado Front Range. *Hydrological Processes* **20**, 2989–3006. doi:10.1002/HYP.6146

Wu Z, Middleton B, Hetler R, Vogel J, Dye D (2015) Vegetation burn severity mapping using Landsat-8 and Worldview-2. *Photogrammetric Engineering and Remote Sensing* **81**(2), 143–154. doi:10.14358/PERS.81.2.143